

# Ant Lion Algorithm for Optimized Controller Gains for Power Quality Enrichment of Off-grid Wind Power Harnessing Units

*Kodakkal Amritha<sup>1</sup>, Veramalla Rajagopal<sup>2\*</sup>, Kuthuri Narasimha Raju<sup>3</sup> and Sabha Raj Arya<sup>4</sup>*

(1. Department of Electrical and Electronics Engineering, BVRIT HYDERABAD College of Engineering for Women, Telangana 500090, India;

2. Department of Electrical and Electronics Engineering, Kakatiya Institute of Technology and Science, Telangana 506015, India;

3. Department of Electrical and Electronics Engineering, Koneru Lakshmaiah Education Foundation, Andhra Pradesh 522502, India;

4. Department of Electrical Engineering, Sardar Vallabhbhai National Institute of Technology Surat, Gujarat 395007, India)

**Abstract:** The proposed system uses an algorithm that works on the admittance of the system, for estimating the reference values of generated currents for an off-grid wind power harnessing unit (WPHU). The controller controls the voltage and maintains the frequency within the limits while working with both linear and nonlinear loads for varying wind speeds. The admittance algorithm is simple and easy to implement and works very efficiently to generate the triggering signals for the controller of the WPHU. The wind power harnessing unit comprising of a squirrel cage induction generator, a star-delta transformer, a battery storage system and the control unit are modeled using Matlab/Simulink R2019. An isolated transformer with a star-delta configuration connects the load and the generator circuit with the controller to reduce the dc bus voltage and mitigate current in the neutral line. The response of the system during the dynamic loading depends on the best possible compensator proportional-integral (PI) gains. The antlion optimization algorithm is compared with particle swarm optimization and grey wolf optimization and is found to have the advantages of good convergence, high efficiency and fast calculating speed. It is therefore used to extract the optimal values of frequency and voltage PI gains. The simulation results of the control algorithm for the WPHU are validated in a real-time environment in a dSpace1104 laboratory set up. This algorithm is proven to have a quick response, maintain the required frequency, suppress the current harmonics, regulate voltage, help in balancing the load and compensating for the neutral current.

**Keywords:** Wind power harnessing unit, induction generator, admittance based control algorithm, ant lion optimization algorithm, voltage and frequency control, battery energy storage system

## 1 Introduction

Wind energy, because of its environment friendliness, availability and cleanliness, has become the most promising renewable energy source. For the past decade, the global wind power industry has experienced enormous growth. The wind power's eco-friendly nature, low carbon emissions, and the cost-effectiveness makes it the most sought-after distributed energy source. The global energy demand

is forecasted to rise by 48% by 2040. Over the next 25 years, 60% of the installed generation will be from zero-emission energy sources, in which solar and wind will contribute 64% of the 8 600 GW increased capacity. In recent years, many major countries have been infusing money to increase the capacity of their installed wind power units, which is a clear indication of the overgrowing demand of this industry. It is estimated that, by 2025, wind energy units will contribute 16% of the world's electricity.

India ranks fourth on the Renewable Energy Country Attractiveness Index, with China on the top

followed by the USA and France. In the next five years, capital costs for wind energy are expected to shrink by 23%. As old technologies continue to get replaced by new ones, these costs are expected to decrease further. As of October 31, 2019, India's total installed renewable energy capacity is estimated as 83 379 MW, of which wind and solar segments accounted for 37 090 MW and 31 696 MW respectively.

Wind power harnessing systems consist of wind turbines, generators, controllers and interconnecting devices. The wind turbine is the basic device in the wind power harnessing system and this acts as a prime mover to rotate the generator. The electrical generator and wind turbine are connected together through a gear train. A controller is introduced in the circuit to minimize disturbances when the generator is loaded, keeping the system parameters within their limits. There can be two modes of operation for wind generators, stand alone or grid connected. In a grid-connected mode, the wind unit supplements the power demanded from the grid. In remote areas where it is not economically viable to extend the grid, the standalone mode is used as an alternative source of electrical power.

The principal aspects of wind power turbines for conversion of energy using an induction generator have been detailed by I Boldia <sup>[1]</sup>. Singh et al. <sup>[2]</sup> reviewed active filters for power quality improvement. Ahmed et al. <sup>[3]</sup> proposed a practical impedance approach for steady-state analysis in the frequency domain for three-phase self-excited induction generators with operating performance evaluations. Lopes et al. <sup>[4]</sup> proposed a fixed-pitch off-grid wind energy conversion system for regulation of voltage and frequency for a self-excited squirrel-cage induction machine and connected voltage source inverter with a controllable dump and battery bank included on the dc side of the voltage source inverter. Jou et al. <sup>[5]</sup> developed a three-phase four-wire power filter comprising a zig-zag transformer and demonstrated its performance under limited zero sequence utility voltage. Lu et al. <sup>[6]</sup> presented an approach to make wind power become a more reliable source in terms of both energy and capacity by using energy storage devices. Combining the wind power generation system with energy storage will reduce fluctuations of

produced energy from wind power. Kou et al. <sup>[7]</sup> presented a new nonlinear model predictive control scheme for the wind farm frequency response. Chauhan et al. <sup>[8]</sup> addressed voltage regulating schemes for self-excited induction generators and summarized their operational aspects and relative suitability. Goel et al. <sup>[9]</sup> focused on an isolated wind-hydro hybrid generation system employing two squirrel-cage induction generators, one driven by a variable-speed system and the other driven by a constant-power system utilizing two back-to-back connected voltage source converters with a battery energy storage system at their DC link. Singh et al. <sup>[10]</sup> presented a conductance-based control algorithm for voltage and frequency control of an isolated induction generator in a small hydro-power system with neutral current compensation. Khadkikar et al. <sup>[11]</sup> devoted a study to emerging power quality problems and state-of-the art solutions. Sakkourya et al. <sup>[12]</sup> investigated the dynamic performance of a self-excited induction generator during startup, and also during increasing or decreasing load. Tawfiq et al. <sup>[13]</sup> performed a comparative review of wind energy conversion system topologies and converters. Psarros et al. <sup>[14]</sup> studied and shed light on the operation of battery-based hybrid power stations in small island systems and their investment feasibility. Kumar et al. <sup>[15]</sup> proposed an algorithm based on quasi-oppositional harmony search. In this study, they compared their algorithm with other algorithms for optimal dynamic performance of load frequency control for diesel-tidal hybrid power generation. Pathak et al. <sup>[16]</sup> developed a renewable wind-hydro system to demonstrate a least-mean-square with reweighted control approach for solutions in power quality. Naidu et al. <sup>[17-18]</sup> discussed a modified enhanced phase-locked loop and sliding mode observer control algorithm for a dynamic voltage restorer with optimization of proportional-integral (PI) gains using particle swarm optimization (PSO) and Harris Hawks optimization algorithms for problems in power quality. The ant colony algorithm was explored for studying ant behavior for optimizing and solving the traveling salesman problem in Ref. [19].

Mirjalili <sup>[20]</sup> introduced the ant lion technique and validated 29 test cases, proving that this algorithm

provides the optimum solution for almost all optimization problems. Two ship propellers were optimized by ant lion optimization (ALO) and compared with other algorithms in terms of improved exploration, convergence and exploitation. It was found that out of the many algorithms available, ALO can effectively avoid local optima and approximate global optima very quickly. Mirjalili [20] compared results from running this algorithm with that of many swarm-based and evolutionary techniques by running all these in test functions. The results very clearly show the supremacy of the ant lion algorithm in terms of stability and significance.

Kushwaha et al. [21] proposed an intelligent sensor for variable wind speed using a maximum- power-point-tracking based Q-learning algorithm. Reddy et al. [22-25] applied an efficient evolutionary algorithm, efficient multi-objective optimization, glowworm swarm optimization and a harmony search algorithm to obtain an optimal power flow solution. Wang et al. [26] presented a review of the emerging strategies to control and improve power quality for grids with connected renewable sources with inverters. Jin et al. [27] suggested an optimization model of a wind-farm collector circuit based on the minimum impedance condition and optimized economic aspects.

In this study, the ant lion algorithm is used for optimizing the values of proportional and integral gains, and the best possible values are obtained in just 10 iterations. This algorithm is theoretically compared with the hydrological cycle algorithm [28], which is one of the most advanced algorithms and is found that the ALO technique is equally robust. Because fewer parameters to be updated, the ant lion algorithm is less complex compared to hydrological cycle algorithm.

## 2 Wind energy background

The power harnessed from wind is directly proportional to the cube of the wind speed and the square of the turbine radius. The efficiency of the wind power harnessing unit (WPHU) is determined by the amount of kinetic energy finally getting converted into electrical power.

It is impossible to convert the all the harnessed

wind power to electrical energy because of various constraints in generator engineering and wind availability, the latter of which depends upon the weather and location. At present, the efficiency of wind power units has been improved to 45% because of developments in technology.

The variation in turbine output power with the change in turbine speed for different wind speeds for zero pitch angle is shown in Fig. 1.

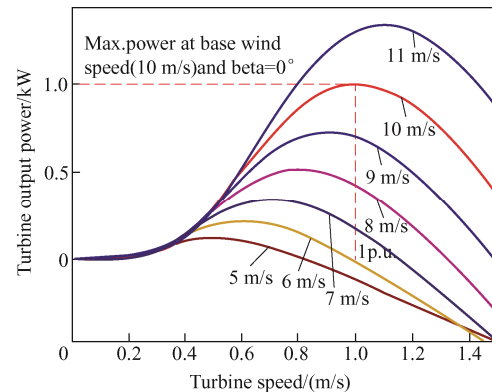


Fig. 1 Variation in turbine output power (7.5 kW) with wind speed

When the wind speed is low, the turbine speed is less and the output power generated is less. Similarly, when the wind speeds are high, turbine speed is high and output power increases. After the maximum power point is reached, any further increase in turbine speed decreases the output power.

## 3 System design

The wind energy conversion system under consideration consists of a four-pole asynchronous generator with a rating of 7.5 kW working with 415 V and 50 Hz. It is configured with a delta connected excitation capacitor of 8 kVA reactive. The schematic diagram of the WPHU is shown in Fig. 2.

A star-delta transformer is employed in the system, through which the controller is connected to the system. The primary winding is selected to handle a voltage of 240 V. The turns ratio is selected in such a way that it acts as a step down transformer to reduce the voltage of the battery at the dc link, and the transformer neutral is connected to the load neutral to suppress the neutral current.

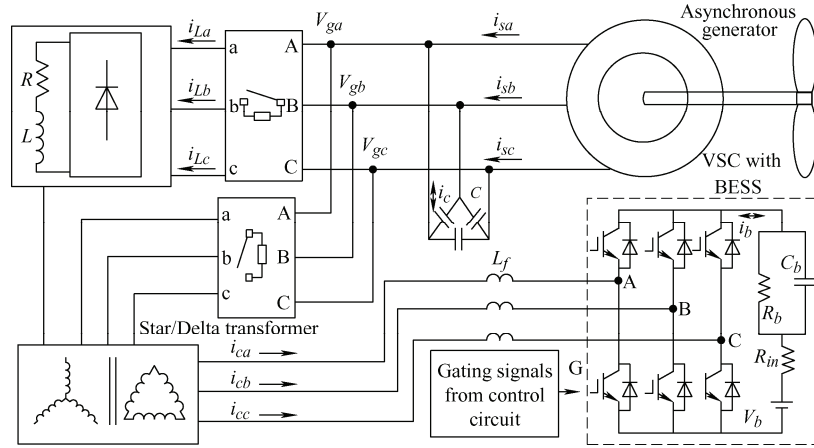


Fig. 2 Schematic diagram of an off grid WPHU

The DC link potential voltage  $V_b$ , which is regulated by the battery, is calculated in terms of the phase voltage  $V_{ph}$  as

$$V_b = 2\sqrt{2} V_{ph} \quad (1)$$

A synchronous speed test gives the value of excitation capacitor, which provides the necessary reactive power required for power generation.

The ac inductor  $L_f$  is designed depending upon the peak-to-peak value of permissible ripple current  $i_p$ , switching frequency  $f$  and the dc bus potential  $V_b$ . The inductance value is calculated as

$$L_f = \frac{\sqrt{3} m V_b}{12 a f i_p} \quad (2)$$

where  $m$  is the modulation index,  $a$  is the overloading factor. Given  $m = 1$ ,  $V_b = 400$  V,  $a = 1.2$ ,  $i_p = 5\%$ , and

$f = 10$  kHz, the inductance value is 2.2 mH.

### 4 Control algorithm

Fig. 3 shows the detailed algorithm explaining the control action of the controller for the suggested system. In this control scheme, the reference source currents are generated based on the admittance algorithm for the system. The related equations are derived as given in the following.

#### 4.1 Computation of in-phase reference currents

The potential at the point of common coupling is calculated by measuring and filtering the three-phase voltages ( $V_{ga}$ ,  $V_{gb}$  and  $V_{gc}$ ) and computing the amplitude as

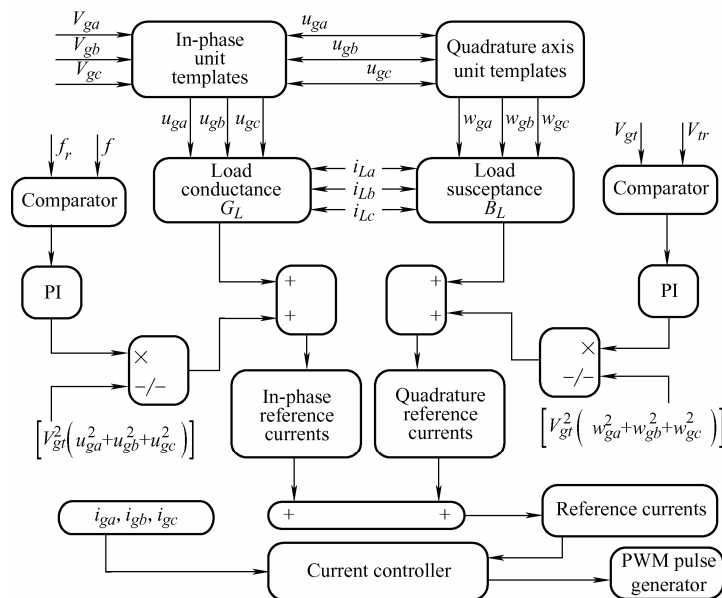


Fig. 3 Control algorithm flowchart

$$V_{gt} = \sqrt{\frac{2}{3}(V_{ga}^2 + V_{gb}^2 + V_{gc}^2)} \quad (3)$$

$u_{ga}$ ,  $u_{gb}$  and  $u_{gc}$  are the unit templates in phase with phase voltages  $V_{ga}$ ,  $V_{gb}$  and  $V_{gc}$ . These are derived as

$$u_{ga} = \frac{V_{ga}}{V_{gt}} \quad u_{gb} = \frac{V_{gb}}{V_{gt}} \quad u_{gc} = \frac{V_{gc}}{V_{gt}} \quad (4)$$

The in-phase reference values of generated currents are determined based on the output signal of the PI controller after duly comparing the measured value of frequency  $f$  with the reference frequency value  $f_r$ .

The frequency error at the  $j^{\text{th}}$  sampling instant is

$$f_{e(j)} = f_{r(j)} - f_{(j)} \quad (5)$$

The PI controller works on this error signal, and the output at the  $j^{\text{th}}$  sampling instant is expressed as

$$P_{d(j)} = P_{d(j-1)} + K_{pd}(f_{e(j)} - f_{e(j-1)}) + K_{id}f_{e(j)} \quad (6)$$

where  $P_{d(j)}$  is the active source power at the  $j^{\text{th}}$  instant.  $K_{pd}$  is the proportional gain and  $K_{id}$  is the integral gain for the PI controller.

The conductance of the controller,  $G_{dc}$  is calculated as

$$G_{dc} = \frac{P_d}{[V_{gt}^2(u_{ga}^2 + u_{gb}^2 + u_{gc}^2)]} \quad (7)$$

The instantaneous load active power  $P_L$  is given by

$$P_L = [V_{gt}(u_{ga}i_{La} + u_{gb}i_{Lb} + u_{gc}i_{Lc})] = P_{Ldc} + P_{Lac} \quad (8)$$

where  $P_L$  is the load active power, consists of two components:  $P_{Ldc}$  is the dc component and  $P_{Lac}$  is the ac component. A low-pass filter is used to extract the dc component of the true power  $P_{Ldc}$ .

The load conductance,  $G_L$  can be given by

$$G_L = \frac{P_{Ldc}}{[V_{gt}^2(u_{ga}^2 + u_{gb}^2 + u_{gc}^2)]} \quad (9)$$

The conductance of the system,  $G_s$  is given as

$$G_s = G_{dc} + G_L \quad (10)$$

In-phase reference components of generated currents are given as

$$\begin{cases} i_{sap} = G_s V_{gt} u_{ga} \\ i_{sbp} = G_s V_{gt} u_{gb} \\ i_{scp} = G_s V_{gt} u_{gc} \end{cases} \quad (11)$$

#### 4.2 Computation of quadrature component of reference currents

The unit quadrature components of voltages  $V_{ga}$ ,

$V_{gb}$  and  $V_{gc}$  are derived from in-phase unit voltages  $u_{ga}$ ,  $u_{gb}$  and  $u_{gc}$  as

$$\begin{cases} w_{ga} = \frac{-u_{gb}}{\sqrt{3}} + \frac{u_{gc}}{\sqrt{3}} \\ w_{gb} = \frac{\sqrt{3}}{2}u_{ga} + \frac{u_{gb}}{2\sqrt{3}} - \frac{u_{gc}}{2\sqrt{3}} \\ w_{gc} = \frac{-\sqrt{3}}{2}u_{ga} + \frac{u_{gb}}{2\sqrt{3}} - \frac{u_{gc}}{2\sqrt{3}} \end{cases} \quad (12)$$

The comparison between the reference value with the measured value of the terminal voltage at the  $j^{\text{th}}$  sampling instant generates the voltage error and is given as

$$V_{gte(j)} = V_{gr(j)} - V_{gt(j)} \quad (13)$$

where  $V_{gr(j)}$  is the reference value of the potential at the point of common coupling (PCC) and  $V_{gt(j)}$  is the magnitude of the ac voltages sensed at the generator terminals at the  $j^{\text{th}}$  instant.

The reactive output power from the PI controller at the  $j^{\text{th}}$  sampling instant required for maintaining a constant potential at ac terminal is given as

$$Q_{V(j)} = Q_{V(j-1)} + K_{pt}(V_{gte(j)} - V_{gte(j-1)}) + K_{it}V_{gte(j)} \quad (14)$$

where  $K_{pt}$  is the proportional gain constant,  $K_{it}$  is the integral gain constant.  $V_{gte(j)}$  is the voltage error in the  $j^{\text{th}}$  instant,  $V_{gte(j-1)}$  is the voltage error in the  $(j-1)^{\text{th}}$  instant and  $Q_{V(j-1)}$  is the reactive power at the  $(j-1)^{\text{th}}$  instant.

The susceptance of the controller  $B_c$  is given as

$$B_c = \frac{Q_V}{[V_{gt}^2(w_{ga}^2 + w_{gb}^2 + w_{gc}^2)]} \quad (15)$$

The instantaneous load reactive power  $Q_L$  is given as

$$Q_L = -[V_{gt}(w_{ga}i_{La} + w_{gb}i_{Lb} + w_{gc}i_{Lc})] = Q_{Ldc} + Q_{Lac} \quad (16)$$

where  $Q_L$  has two components:  $Q_{Ldc}$  is the dc component, showing the average value;  $Q_{Lac}$  is the ac component, indicating the oscillating nature. A low pass filter is used to pull out the dc component  $Q_{Ldc}$  of the load reactive power.

The susceptance of the load,  $B_L$  is determined using the Eq. (17)

$$B_L = \frac{V_{gt}^2(w_{ga}^2 + w_{gb}^2 + w_{gc}^2)}{Q_{Ldc}} \quad (17)$$

The total susceptance,  $B_s$  is given by

$$B_s = B_c - B_L \quad (18)$$

where  $B_c$  and  $B_L$  are the susceptances of the controller

and the load respectively.

The quadrature reference components of generated currents are calculated as

$$\begin{cases} i_{gaq} = B_s V_{gt} W_{ga} \\ i_{gbq} = B_s V_{gt} W_{gb} \\ i_{gcq} = B_s V_{gt} W_{gc} \end{cases} \quad (19)$$

#### 4.3 Calculation of reference generator currents

The reference generator currents are estimated as

$$\begin{cases} i_{ga}^* = i_{gap} + i_{gaq} \\ i_{gb}^* = i_{gbp} + i_{gbq} \\ i_{gc}^* = i_{gcp} + i_{scq} \end{cases} \quad (20)$$

The reference generator currents  $i_{ga}^*$ ,  $i_{gb}^*$  and  $i_{gc}^*$  and sensed generator currents  $i_{ga}$ ,  $i_{gb}$  and  $i_{gc}$  are fed as inputs to the comparator, which compares both to output an error value. This current error is applied to a hysteresis current controller, which generates the triggering signals for the insulated gate bipolar transistors in the voltage source converter.

### 5 Optimization of PI gains using the antlion algorithm

The ALO algorithm was used for optimizing the values of PI gains of the frequency and voltage controllers. This algorithm mimics interaction between ant lions and ants in a trap.

Ants exhibit random movement in nature while searching for food and this movement can be modeled as

$$X(t) = \begin{bmatrix} 0, cs(2r(t_1)-1), cs(2r(t_2)-1), \\ cs(2r(t_3)-1), \dots, cs(2r(t_{iter\_max})-1) \end{bmatrix} \quad (21)$$

where  $cs(\cdot)$  computes the integral sum,  $iter\_max$  is the iteration size,  $t$  is the random walk step and  $r(t)$  is a function given by

$$r(t) = \begin{cases} 1 & \text{if } rand > 0.5 \\ -1 & \text{if } rand \leq 0.5 \end{cases} \quad (22)$$

$Matrix_{Ant}$  is used for saving and utilizing each ant position for optimization, which can be expressed as

$$Matrix_{Ant} = \begin{bmatrix} A_{(1,1)} & A_{(1,2)} & \dots & A_{(1,m)} \\ A_{(2,1)} & A_{(2,2)} & \dots & A_{(2,m)} \\ \vdots & \vdots & & \vdots \\ A_{(n,1)} & A_{(n,2)} & \dots & A_{(n,m)} \end{bmatrix} \quad (23)$$

$A(n,m)$  shows the value of  $m^{th}$  variable of  $n^{th}$  ant; 'n' is the number of ants, and 'm' is the number of variables.

An objective function is used for evaluating each ant fitness for the given optimization period. The entire set of ant fitness values are stored in  $Matrix_{OA}$ , which can be expressed as

$$Matrix_{OA} = \begin{bmatrix} f([A_{(1,1)}, A_{(1,2)}, \dots, A_{(1,m)}]) \\ f([A_{(2,1)}, A_{(2,2)}, \dots, A_{(2,m)}]) \\ \vdots \\ f([A_{(n,1)}, A_{(n,2)}, \dots, A_{(n,m)}]) \end{bmatrix} \quad (24)$$

Antlions are hiding somewhere apart from ants lying in the search space.

$Matrix_{Antlion}$  is obtained to save and utilize every antlion position, which can be expressed as

$$Matrix_{Antlion} = \begin{bmatrix} AL_{1,1} & AL_{1,2} & \dots & AL_{1,m} \\ AL_{2,1} & AL_{2,2} & \dots & AL_{2,m} \\ \vdots & \vdots & & \vdots \\ AL_{n,1} & AL_{n,2} & \dots & AL_{n,m} \end{bmatrix} \quad (25)$$

where  $AL(n, m)$  shows the value of  $m^{th}$  variable of  $n^{th}$  ant;  $n$  is the number of ants;  $m$  is the number of variables.

An objective function is used to evaluate the fitness of each antlion for the period of optimization and the entire set of antlion fitness values are stored in  $Matrix_{OAL}$ , which can be expressed as

$$Matrix_{OAL} = \begin{bmatrix} f([AL_{1,1}, AL_{1,2}, \dots, AL_{1,m}]) \\ f([AL_{2,1}, AL_{2,2}, \dots, AL_{2,m}]) \\ \vdots \\ f([AL_{n,1}, AL_{n,2}, \dots, AL_{n,m}]) \end{bmatrix} \quad (26)$$

To keep the variable in the search space, the positions are been normalized for optimization during each step of random walk and given as

$$X_i^t = \left( \frac{X_i^t - a_i}{d_i^t - a_i} \right) (d_i - c_i^t) + c_i \quad (27)$$

where  $a_i$  is the minimum random walk of the  $i^{th}$  variable.  $c_i$  and  $d_i$  are the minimum and maximum respectively of  $i^{th}$  ant.  $c_i^t$  and  $d_i^t$  are the minimum and maximum of the  $i^{th}$  ant at the  $t^{th}$  iteration.

$$\begin{cases} c'_i = c^t + Antlion'_j \\ d'_i = d^t + Antlion'_j \end{cases} \quad (28)$$

where  $c^t$  and  $d^t$  are the vectors indicating minimum and maximum of whole variables at the  $t^{th}$  iteration.  $Antlion'_j$  is the position of  $j^{th}$  antlion at the  $t^{th}$  iteration.

The decreasing behavior that mimics the process of sliding of ants inside the pits is given by

$$c^t = \frac{c^t}{10^w (t / iter\_max)} \quad d^t = \frac{d^t}{10^w (t / iter\_max)} \quad (29)$$

The equation for updating the position to the latest by the hunted ant to enhance its chance of catching new prey is

$$Antlion'_j = Ant'_i \quad \text{if } f(Ant'_i) < f(Antlion'_j) \quad (30)$$

where  $Ant'_i$  is the position of  $i^{th}$  ant at the  $t^{th}$  iteration.

The fittest antlion is known as the elite. Each ant randomly walks around an antlion selected by the roulette wheel, and the elite concurrently, which can be expressed as

$$Ant'_i = \frac{R'_A + R'_E}{2} \quad (31)$$

where  $R'_A$  and  $R'_E$  are the random walks around the antlion selected by the roulette wheel, and the elite respectively, for the  $i^{th}$  ant at  $t^{th}$  iteration.

The cost function is an optimization problem of minimizing the steady state errors of frequency PI controller  $PI_1$  and ac voltage PI controller  $PI_2$ .

The cost function is given by

$$O = w_1 \times ISTE_1 + w_2 \times ISTE_2 \quad (32)$$

where  $w_1$  and  $w_2$  are the weights of  $ISTE_1$  and  $ISTE_2$  and are taken as 0.5.  $ISTE_1$  and  $ISTE_2$  are the inputs to frequency and ac PI controllers.

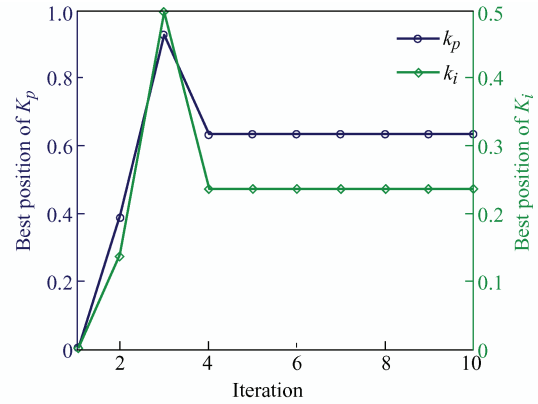
The Simulink model workspace data ( $ISTE_1$  and  $ISTE_2$ ) are extracted and then given to the ALO algorithm for optimizing PI gains.

From Eq. (6) and Eq.(14), it can get

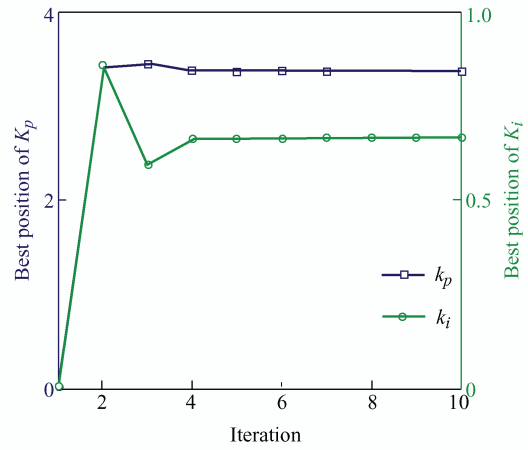
$$\begin{aligned} \text{Cost function} = & 0.5 \{ P_{d(j-1)} + K_{pd} (f_{e(j)} - f_{e(j-1)}) + K_{id} f_{e(j)} \} + \\ & 0.5 \{ Q_{v(j-1)} + K_{pv} \{ V_{gve(j)} - V_{gve(j-1)} \} + K_{iv} V_{gve(j)} \} \end{aligned} \quad (33)$$

Figs. 4a and 4b show optimum gains of  $K_p$  and  $K_i$  for both frequency and AC controllers at 0.661, 0.235,

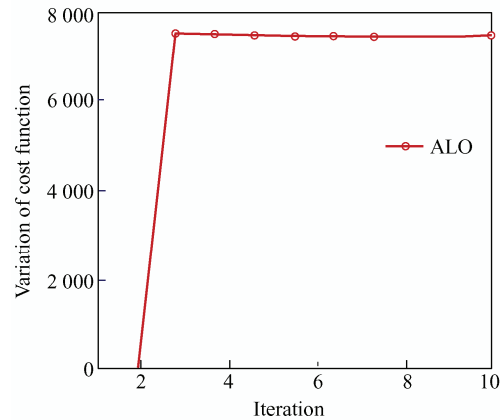
3.350 and 0.633, in 10 iterations. It can be seen from the ALO algorithm convergence curve (Fig. 4c) that the cost function converges at 7 525.



(a) Trajectory of AC-PI gains



(b) Trajectory of Freq-PI gains



(c) Convergence curve

Fig. 4 Trajectory and convergence curve of PI gains of ALO algorithm

Figs. 5a-5c show optimum gains of  $K_p$  and  $K_i$  for both frequency and AC controllers. The cost function converges at -1.26, 7.66, 6.39, -1.06 and 1 761.12 in 10 iterations.

Figs. 6a-6c show optimum gains of  $K_p$  and  $K_i$  for

both frequency and AC controllers and cost function converges at 0.14, 4.63, 2.13, 1.05 and 1 761.12 in 10 iterations.

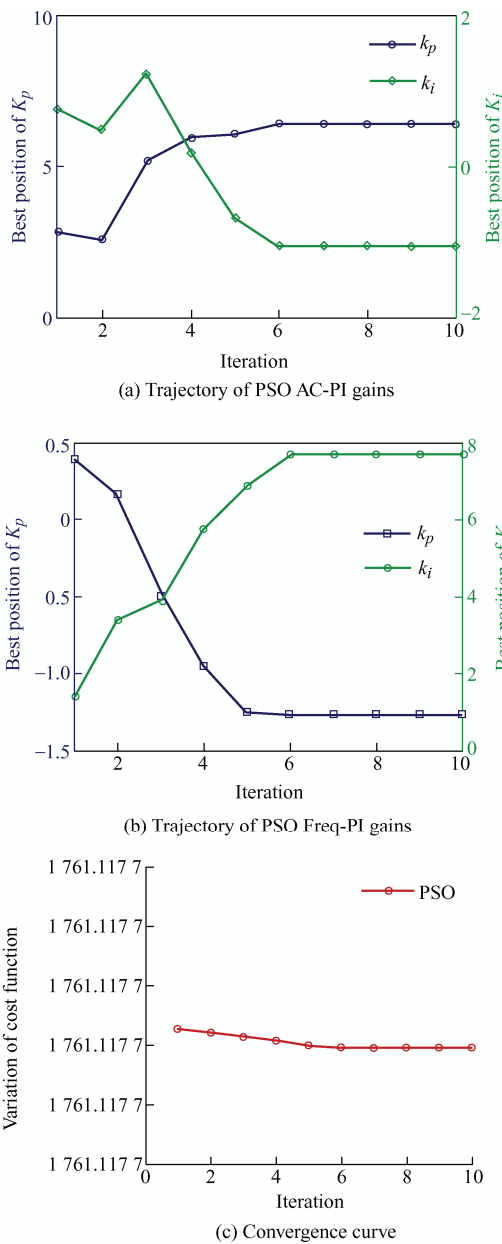


Fig. 5 Trajectory and convergence curve of PI gains of the PSO algorithm

The ALO algorithm was compared with the PSO algorithm and grey wolf optimization for an off grid WPHU for optimizing proportional and integral gains of frequency PI and the ac voltage PI controllers. It can be seen that PSO and grey wolf optimization algorithm  $K_p$  and  $K_i$  values are not giving proper results. The obtained values when applied to an off grid WPHU are not exhibiting satisfactory results for power quality and system dynamics.

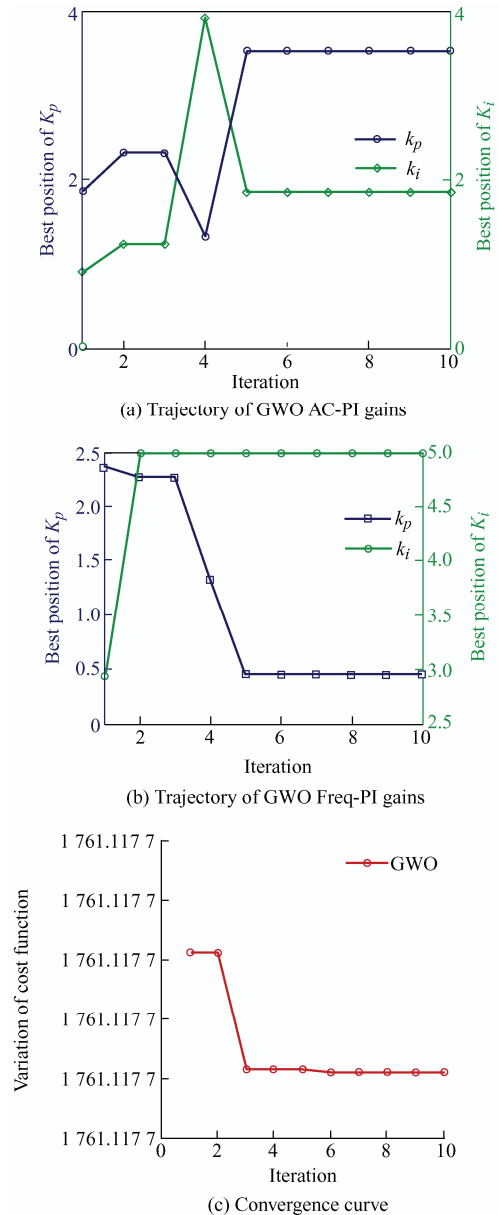


Fig. 6 Trajectory and convergence curve of PI gains of the grey wolf optimization algorithm

## 6 Simulation results

A WPHU using an induction generator was simulated in Matlab/Simulink using the Sim-Power System tool box. The load current, source current, terminal voltage developed, and frequency were observed at different time intervals under different load and wind conditions. The wind generating unit started developing a voltage at 0.3 s with a load connected at 0.35 s and a controller connected at 0.5 s to the system. The proposed algorithm was applied for both linear and nonlinear loading circuits; in both cases, voltage and frequency regulation was obtained swiftly. The load in one of the phases was



disconnected at 4.65 s, and thus, an imbalance was created; the same load was again applied at 4.75 s. The controller acted quickly to restore balance in the source circuit currents during 4.65-4.75 s. The controller maintained the voltage and frequency regulation of the system.

Fig. 7 shows the waveforms of source voltage, source current, load current and compensating current, terminal voltage, frequency, battery current, load neutral current, source neutral current, and wind speed of the generator-turbine set with nonlinear loads at constant wind speed.

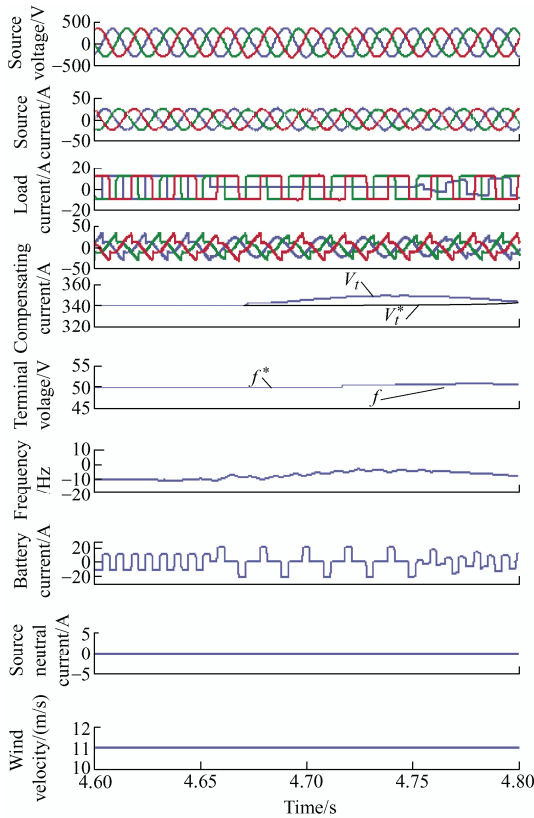


Fig. 7 Performance of the WPHU with nonlinear loads at constant wind speed

When one phase of the load was removed at 4.65 s and reconnected at 4.75 s, the source currents were balanced during balanced and unbalanced load conditions. In both the above cases, during the time of load imbalance, it is found that the battery current is positive, which is an indication that the battery is in the charging mode. The battery absorbs the extra amount of power, which helps in maintaining constant voltage and frequency.

Fig. 8a shows a schematic of a star-delta transformer. Fig. 8b shows the simulation results of

source current at phase a, load current at phase a, and neutral current flows between the load and star-delta transformer, indicating the compensation of multiples of third harmonics and zero sequence currents.

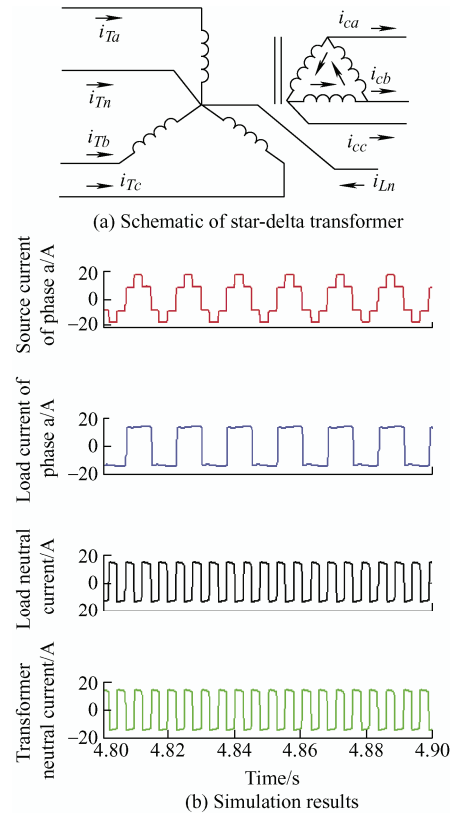
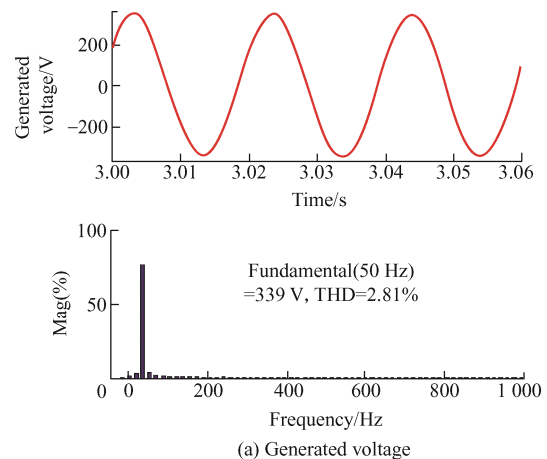


Fig. 8 Star-delta transformer for compensation of neutral current

The three waveforms in Figs. 9a-9c show the total harmonic distortion (THD) values of the source voltage, source current and load current respectively, with a nonlinear load. The THD values of the source voltage, source current, and load current were found to be 2.81%, 4.77%, and 38.85%, respectively, all of which are well within their operating limits according to IEEE 519 standards.



(a) Generated voltage

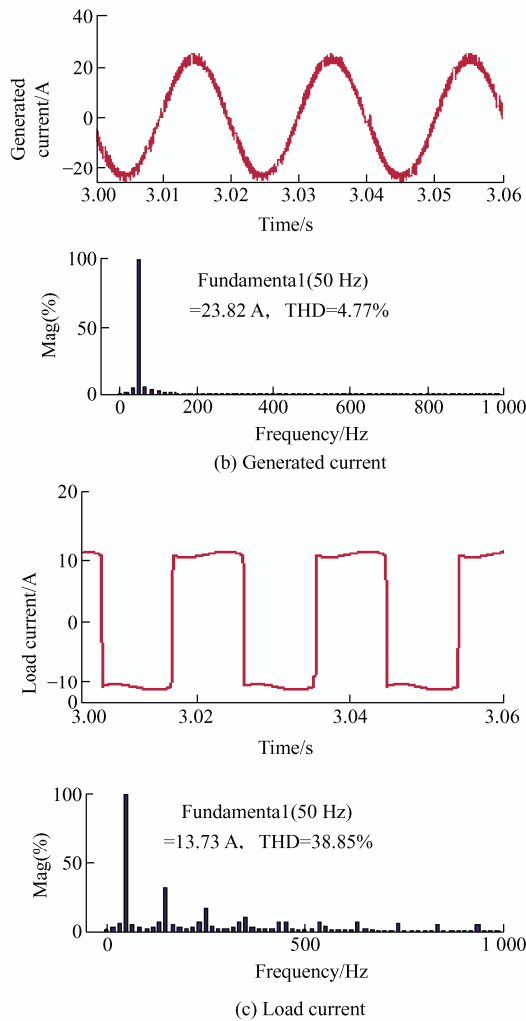


Fig. 9 THD in generated voltage, generated current and load current

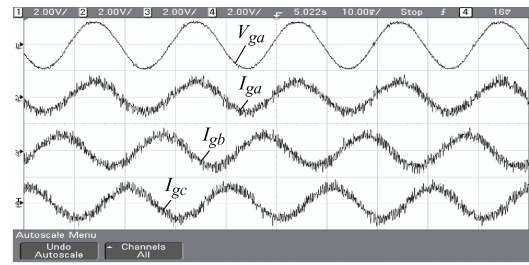
### 7 Hardware results

The admittance control algorithm that uses the ALO PI controller gains was tested on a hardware prototype. The set-up used a DS1104 controller board that included a digital signal processing microcontroller (TMS320F240) which acts as a slave digital signal processor. The results were illustrated using a single-phase power quality analyzer (Fluke 43B), which records the steady-state performance and a digital signal oscilloscope, which captures the dynamic performance.

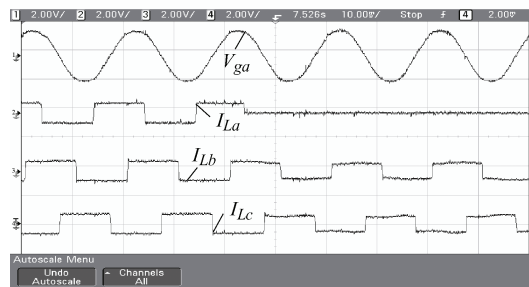
Figs. 10a-10c show the results of the phase a source voltage with three-phase source currents, three-phase load currents and three-phase controller currents respectively, captured during a real time environment during the load imbalance. Fig. 10d depicts the captured results of the phase a source voltage with single-phase source current, single-phase load current and single-phase controller current.

Fig. 10e shows the results of the phase a source voltage with single-phase source current, load current, and load neutral current. Fig. 10f shows the results of the phase a source voltage with single-phase source current, load current, and source neutral current.

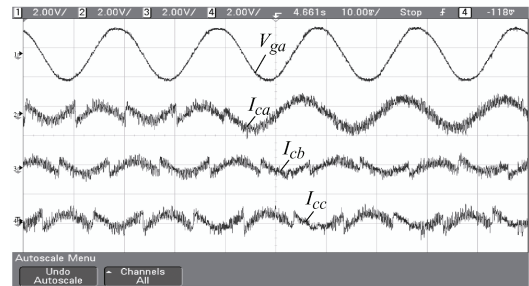
It can be seen that the experimental results match with the simulation results in keeping the source currents sinusoidal and balanced during load removal. The neutral current of the source is zero, even when neutral current of the load is non-zero which exhibits the neutral current compensation of the star-delta transformer.



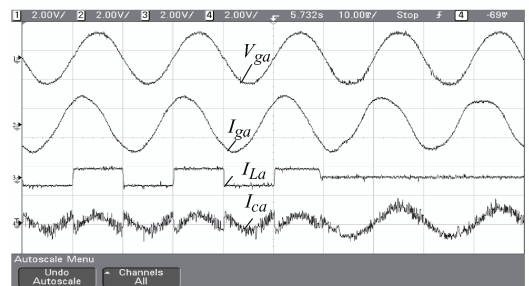
(a) Phase a generator voltage and three-phase generator currents when the load is unbalanced



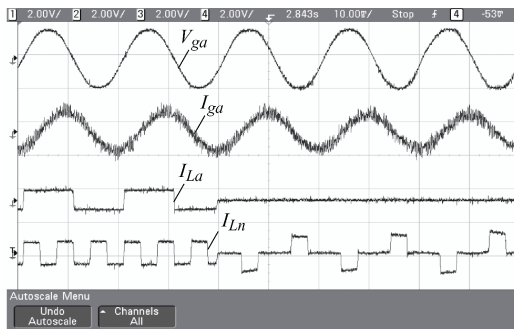
(b) Phase a generator voltage and three-phase load currents when the load is unbalanced



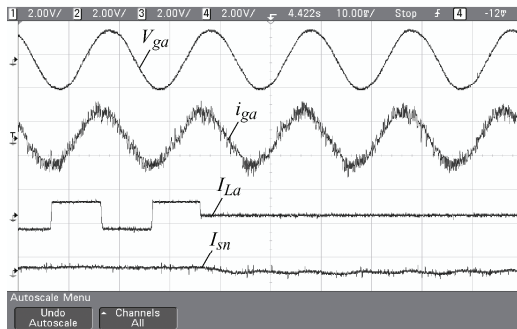
(c) Phase a generator voltage and three-phase compensator currents when the load is unbalanced



(d) Phase a generator voltage, generator current, load current and compensator current when the load is unbalanced



(e) Phase a generator voltage, generator current, load current and neutral current during load unbalance



(f) Phase a generated voltage, generated current, load current and source neutral current when the load is unbalanced

Fig. 10 Hardware results

## 8 Conclusions

The control of real and reactive powers for WPHUs with the proposed algorithm is simulated using Matlab/Simulink and validated on a real-time prototype DS1104 hardware setup. The resultant waveforms under imbalance and different wind conditions are observed and studied. Three optimization algorithms are compared; ALO, PSO and grey wolf optimization. It is found that the most optimized values for PI gains are obtained from the ALO algorithm. The admittance algorithm maintains the sinusoidal shapes for the source current waveform with terminal voltage and frequency well within the limits under unbalanced load conditions and changing wind speeds. The THD is less than 5%. It is concluded that the admittance control algorithm with ALO incorporated in it, is very effective in power quality improvement.

## References

- [1] I Boldia. Variable speed generator: The electrical generator handbook. New York: Taylor & Francis, 2006.
- [2] B Singh, K Al-Haddad, A Chandra. A review of active

filters for power quality improvement. *IEEE Transactions on Industrial Electronics of Power Electronics*, 1999, 46(5): 960-971.

- [3] T A E Ahmed, O Noro, E Hiraki, et al. Terminal voltage regulation characteristics by static var compensator for a three-phase self-excited induction generator. *IEEE Transactions Industrial Applications*, 2004, 40(4): 978-988.
- [4] L Lopes, R G Almeida. Wind-driven self excited induction generator with voltage and frequency regulated by a reduced rating voltage source inverter. *IEEE Transactions on Energy Conversion*, 2006, 21(2): 297-304.
- [5] H L Jou, K D Wu, J C Wu, et al. A three-phase four-wire power filter comprising a three-phase three-wire active power filter and a zig-zag transformer. *IEEE Transactions on Power Electronics*, 2008, 23(1): 252-259.
- [6] M S Lu. Combining the wind power generation system with energy storage equipment. *IEEE Transactions Industrial Applications*, 2009, 45(6): 2109-2115.
- [7] P Kou, D Liang, L B Yu, et al. Nonlinear model predictive control of wind farm for system frequency support. *IEEE Transactions on Power Systems*, 2019, 34(5): 3547-3561.
- [8] Y K Chauhan, S K Jain, B Singh. A prospective on voltage regulation of self-excited induction generators for industry applications. *IEEE Transactions on Industry Applications*, 2010, 46(2): 720-730.
- [9] P K Goel, B Singh, S S Murthy. Isolated wind-hydro hybrid system using cage generators and battery storage. *IEEE Transactions on Industrial Electronics*, 2011, 58(4): 1141-1153.
- [10] B Singh, V Rajagopal. Digital control of voltage and frequency of induction generator in isolated small hydro system. *Proceedings of IEEE International Conference on Power Electronics, Drives and Energy Systems (PEDES)*, 2012: 1-7.
- [11] V Khadkikar, D G Xu, C Cecati. Emerging power quality problems and state-of-the-art solutions. *IEEE Transactions on Industrial Electronics*, 2017, 14(3): 468-477.
- [12] K S Sakkourya, S Emaraa, A M Kamal. Analysis of wind driven self-excited induction generator supplying isolated DC loads. *Journal of Electrical Systems and Information Technology*, 2016: 257-268.
- [13] K B Tawfiq, A S Mansoura, H A Ramadan, et al. Wind energy conversion system topologies and converters: Comparative review. *Energy Procedia*, 2014, 162: 38-47.
- [14] G N Psarros, S Papanthassiou. Evaluation of battery-renewable hybrid stations in small-isolated systems. *IET Renewable Power Generation*, 2020, 14(1):

- 39-51.
- [15] A Kumar, G Shankar. Quasi-oppositional harmony search algorithm based optimal dynamic load frequency control of a hybrid tidal-diesel power generation system. *IET Generation, Transmission & Distribution*, 2018, 12(5): 1099-1108.
- [16] G Pathak, B Singh, K Bijaya. Wind-hydro microgrid and its control for rural energy system. *IEEE Transactions on Industry Applications*, 2019, 55(3): 3037-3045.
- [17] T A Naidu, S R Arya, R Maurya. Multi-objective dynamic voltage restorer with modified EPLL control and optimized PI-controller gains. *IEEE Transactions on Power Electronics*, 2019, 34(3): 2181-2192.
- [18] T A Naidu, S R Arya, R Maurya, et al. Compensation of voltage based power quality problems using sliding mode observer with optimized PI controller gains. *IET Generation, Transmission & Distribution*, 2020, 14(14): 2656-2665.
- [19] A Colomi, M Dorigo, V Maniezzo. Distributed optimization by ant colonies. *Proceedings of the First European Conference on Artificial Life*, 1991: 134-142.
- [20] S Mirjalili. The ant lion optimizer. *Advances in Engineering Software*, 2015, 83: 80-98.
- [21] A Kushwaha, M Gopal, B Singh. Q-learning based maximum power extraction for wind energy conversion system with variable wind speed. *IEEE Transactions on Energy Conversion*, DOI: 10.1109/TEC.2020.2990937.
- [22] S S Reddy, P R Bijwe, A R Abhyankar, et al. Faster evolutionary algorithm based optimal power flow using incremental variables. *International Journal of Electrical Power & Energy Systems*, 2014, 54: 198-210.
- [23] S S Reddy, P R Bijwe. Multi-objective optimal power flow using efficient evolutionary algorithm. *International Journal of Emerging Electric Power Systems*, 2016, 18(2): 1-21.
- [24] S S Reddy, C S Rathnam. Optimal power flow using Glowworm Swarm optimization. *International Journal of Electrical Power & Energy Systems*, 2016, 80: 128-139.
- [25] S S Reddy. Optimal power flow using hybrid differential evolution and harmony search algorithm. *International Journal of Machine Learning and Cybernetics*, 2019, 10: 1077-1091.
- [26] T Wang, H Nian, Z Q Zhu. Using inverter-based renewable generators to improve the grid power quality: A review. *Chinese Journal of Electrical Engineering*, 2018, 4(4): 16-25.
- [27] H Jin, X Y Zhang, Y Zhang, et al. Optimization of wind farm collection line structure under symmetrical grid fault. *Chinese Journal of Electrical Engineering*, 2019, 5(3): 49-58.
- [28] J Whalley, A Narayanan. Hydrological cycle algorithm for continuous optimization problems. *Journal of Optimization*, 2017(10): 1-25.



**Kodakkal Amritha** received her B.E. degree in electrical & electronics engineering from Karnataka Regional Engineering College, Surathkal (presently NIT, Surathkal), and her M.T. in power electronics and industrial drives at JNTUH, Hyderabad, India.

She is working as an associate professor at BVRIT HYDERABAD College of Engineering for Women, Hyderabad. She is currently doing her research at KL Deemed University, in the field of power quality improvement in wind energy conversion systems. Her research interests include power electronic converters, renewable energy sources and power quality.



**Veramalla Rajagopal** received his AMIE (electrical) degree from the Institution of Engineers (India), his M.T. degree from the Uttar Pradesh Technical University, India and his Ph.D degree from the Indian Institute of Technology (IIT), Delhi.

He is presently working as a professor of electrical and electronics engineering, Kakatiya Institute of Technology and Science, Warangal, Telangana, India. His areas of interest include power electronics and drives, renewable energy generation and applications, flexible AC transmission system, and power quality. He holds one patent, has authored 20 international and national journals articles, and has presented at 34 IEEE and national conferences held at India and abroad. He is a life member of the Indian Society for Technical Education (ISTE) and the fellow of Institution of Engineers (India).



**Kuthuri Narasimha Raju** has completed his B.T. at Sri Venkateswara Hindu College of Engineering, Machlipatnam in electrical and electronics engineering in 2002, his M.T. in power electronics and industrial drives at JNTUH in 2012 and his Ph.D from KL Deemed

University in 2018.

He is currently working as a professor in the EEE department and as associate dean of the Internal Quality Assurance Cell at KL deemed University. His research interests include pulse width modulation techniques for switched mode converters, novel multilevel inverter topologies, DC microgrid, electric vehicles and power systems. Presently he is guiding eight research scholars and has successfully supervised eight PG theses. He has been presented with the Uttam Acharya Award for the year 2019 by Indian servers and received the Best Teacher award for academic years 2012-2013 and 2016-2017 at KL Deemed University.



**Sabha Raj Arya** received his B.E. degree in electrical engineering from Government Engineering College, Jabalpur, in 2002, M.T. in power electronics from Motilal National Institute of Technology, Allahabad, in 2004, and Ph.D. degree in electrical engineering from Indian Institute of Technology (IIT) Delhi, New Delhi, India, in 2014. He joined as an assistant professor in the Department of Electrical Engineering, Sardar Vallabhbhai National Institute of Technology, Surat. In January 2019, he was promoted to associate professor in the same institution. His fields of interest include power electronics, power quality, design of power

filters and distributed power generation.

He received two national awards: INAE Young Engineer Award from the Indian National Academy of Engineering and the POSOCO Power System Award from the Power Grid Corporation of India in 2014 for his research work. He has also received the Amit Garg Memorial Research Award in 2014 from IIT Delhi for high impact publications in a quality journal during the session 2013-2014. He has published more than 100 research papers in international journals and conferences in the field of electrical power quality.

He also serves as an associate editor for the IET (UK) *Renewable Power Generation*.